Received 5 April 2024; revised 15 May 2024; accepted 19 May 2024. Date of publication 28 May 2024; date of current version 6 August 2024.

Digital Object Identifier 10.1109/OJAP.2024.3406067

A Mutual Coupling-Based Full Self-Online Calibration Method for Antenna Arrays in Uplink

ARAL ERTUG ZORKUN[1], MIGUEL A. SALAS-NATERA[1], ALVARO ARAUJO PINTO[2], RAMÓN MARTÍNEZ RODRÍGUEZ-OSORIO[1], AND MANUEL SIERRA PÉREZ[1] (Life Senior Member, IEEE)

[1]Centro de Procesamiento de Información y Telecomunicaciones, Escuela Técnica Superior de Ingenieros de Telecomunicación, Universidad Politécnica de Madrid, 28040 Madrid, Spain

[2]Escuela Técnica Superior de Ingenieros de Telecomunicación, Universidad Politécnica de Madrid, 28040 Madrid, Spain

CORRESPONDING AUTHOR: M. A. SALAS-NATERA (e-mail: miguel.salas@upm.es)

This work was supported by the Spanish Government, the Ministry of Economy, and the National Program of Research, Development, and Innovation through the Project New Array Antenna Techlogies and Digital Processing for the FUTURE Integrated Terrestrial and Space-Based Millimeter-Wave Radio Systems, UPM-InTerSpaCE under Grant PID2020-112545RB-C51.

ABSTRACT This paper proposes a mutual coupling based self-calibration method for transmit mode large scale antenna arrays. In accord with the proposed active antenna array model, gain/phase uncertainties, antenna element position errors and mutual coupling effects are reduced to an error matrix. The expansion of equations of the proposed calibration method are presented. The proposed calibration procedure is capable of compensating the error matrix while the system is operating and is suitable for off-line, on-site and online calibration procedures. The calibration procedure relies on the measurements of the error signal related to scan reflection coefficient while the system is operating, and the premeasured inter-element couplings. The calibration system takes pre-measured couplings, the geometry of the antenna array, the antenna weights and pointing direction as input, then, during the operation it combines input with the measured feedback signals to construct an array manifold. The coefficients of the error matrix are later estimated from the array manifold. The antenna weights are compensated by direct inversion of the estimated error matrix which involves division operator, yielding possible inaccurate coefficient estimation in hardware. Therefore, a globally convergent generalized inverse matrix approximation method is adopted. Simulation results with worst case errors and a simple experimental study are presented. The results show that with the proposed method, accurate calibration can be made with couplings only in the first and second order neighbors of an antenna element.

INDEX TERMS Active antenna array, inverse matrix approximation, mutual coupling effect, self-calibration, up-link antenna arrays.

I. INTRODUCTION

LARGE-SCALE phased array antennas are considered to play fundamental role in the fifth-generation (5G) [1], [2] and future sixth-generation (6G) wireless communication systems [3], [4]. The new generation 5G and 6G wireless systems are expected to be used in many civil, commercial, and military areas such as massive multiple-input multiple-output (mMIMO) [5], [6], autonomous driving [7], satellite systems [3], Internet of Things (IoT) [4], anti-jamming, and anti-spoofing [8]. With the latest developments in phased array antenna technology, beamforming is intended to be one of the key techniques for the next generation wireless systems [1], [2], [9]. Beamforming techniques direct the pattern of the antenna array in the desired direction by varying the phase of each antenna element, maximizing signal-to-noise ratio (SNR), compensating for high path losses, distinguishing users, and canceling interference to improve signal quality [2], [9], [10]. Depending on the application, beamforming system architectures can be active, hybrid or fully digital [2]. However, all beamforming architectures contain many radio frequency (RF) components such as amplifiers, phase shifters, filters, analog-to-digital converters (ADC), digital-to-analog converters (DAC) and so forth [11]. Different transfer characteristics of RF

components, mechanical manufacturing errors, aging of components, temperature variations and position errors cause unequal excitation of each antenna element, thus deteriorating the overall performance of the system [7], [11]. Therefore, to avoid system performance loss, the above-mentioned errors must be measured and predicted in advance and the phased array antenna system must be calibrated according to the information obtained before and/or during operation.

In the calibration procedure, signal samples are collected from each antenna element or subarrays and then these signal samples are used to determine the compensation weights [7]. The calibration process of phased antenna arrays, whether transmitting or receiving, are similar to each other except for minor differences [7], [11]. In receive mode, a test signal is injected as the input of each element, a special reference or self-correlation process with a beamformer is required to combine all inputs [12], [13]. On the contrary, in the transmit mode, each element must be excited by a source signal and a combined signal monitoring at the output is required [11], [14], therefore only RF chain information can be obtained or an external sensor is used to receive and monitor the signal from each element. The calibration methods can be divided into four subgroups: the near-field or far-field probing methods (NF-FF-P), the peripheral-fixed probe method (PXP), the mutual (MC) coupling methods and the built-in (BI) network methods [13], [15], [16].

The near-field or far-field probing methods employ a test probe moved across a phased antenna array to measure the relative phase and amplitude of each antenna element [6], [17], [18]. The peripheral fixed probe methods use one or more fixed probes around the periphery of the phased array to measure the coupling between antennas and compensate for excitation errors [19], [20]. Probing methods can be considered on-site calibration methods since the phased antenna array under test must be within the field of view of the test probe/s. In mutual coupling methods, coupling between all pairs of antenna elements is used to characterize the exact relative phase and amplitude errors of each antenna element [16], [21], [22]. Lastly, in built-in network calibration methods, couplers are connected to the terminals of each antenna element in the phased array to sample the reference signal from the radiating element. The received or transmitted signals measured at the connected end are then used to determine phase and amplitude mismatches of the antenna elements [2], [13], [23], [24], [25]. Depending on the application, calibration methods can be used in offline, on-site, or online calibration systems by implementing application specific calibration algorithms and additional hardware [14], [22], [26], [27]. For large-scale antenna arrays fast, self-calibrating and on-line calibration methods are favorable. Also, not using external sub-systems and additional processors for calibrating signals is an advantage.

The near-field or far-field probing methods usually employ rotating-element electric-field vector (REV) method [27], [28], [29]. The REV method is inefficient for large-scale antenna array calibration since the calibration time increased drastically as the number of antennas increases and in particular, near-field probing methods are only suitable for off-line calibration [5], [7]. Moreover, it is difficult to verify the correct combination of signals in the far-field due to the limited feedback path [16]. Therefore, studies in [22], [27], [28], [29] are not suitable for large-scale antenna array calibration. The method in [22] takes into account mutual-couplings, however, the technique depends on the park and probe measurements which is considered as REV. On the other hand, the peripheral-fixed probe methods can be used for on-line calibration [3]. However, they require auxiliary reference antennas for measurement, additional hardware [1], [30] and complex calibration algorithms [26] that increase the system size and complexity [7]. The probing methods are time-consuming and costly, as well as, often require facilities and additional measurement equipment [14], [31], thus, studies in [1], [3], [18], [26], [30], [32] are not suitable for the large-scale antenna array calibration. On the contrary, mutual coupling and built-in network calibration methods can be fast and cost-effective, in fact, they are suitable for on-line calibration.

The mutual coupling methods are capable of performing parallel calibration without adding extra antennas or increasing the system size [7], [16]. However, these methods need complex calibration algorithms [33] because of the stringent requirements for isolation between array elements and the non-uniform regulation of the sensitivity of the antenna elements, resulting in calibration errors in large-scale antenna arrays [5], [7]. In [14], a self-calibration method based on mutual coupling for initial calibration is proposed which is not suitable for on-line calibration. In [34], a mutual coupling based pattern reconstruction method is proposed, this study is impractical for large-scale array calibration since the radiation pattern measurements are time consuming. The study in [8] proposes precise self-calibration method taken into account mutual couplings, however, measurement and calibration systems are highly complex. Moreover, in [16], a calibration method based on active antenna element pattern taking into account mutual couplings is proposed. The proposed calibration method is robust; however, it is not suitable for on-line self-calibration.

The built-in network calibration methods are highly accurate and efficient, moreover, calibration of multiple elements can be performed in parallel without the need for consistent measurements [7]. The built-in network calibration methods require coupled lines for the feedback signals, however, as the number of antennas increased, the number of coupled lines also increases, resulting in possible coupling errors between the lines [24], [35], [36]. Moreover, the built-in network calibration methods require closed-loop testing and might not be suitable for on-line calibration as in [13]. In [2], a built-in on-line self-calibration is proposed, however, the mutual couplings are not taken into account, thus, for large-scale antenna arrays there might be calibration errors. In [5],

TABLE 1. Comparison of the discussed calibration methods from the literature.

Ref.	Year	Method Classification	Used Technique for the Calibration	Highlights	Required Measurements	Mode
[32]	2013	NF-FF-P	Orthogonal coded signals	-Compensated Errors: Amp., Phase -Suitable Application: Off-line, On-site, Self-cal.	Power	Tx
[34]	2014	MC	Element pattern reconstruction	-Compensated Errors: MC -Suitable Application: Off-line, On-site, Online, Self-cal..	Pattern	Rx
[8]	2014	MC	Iterative algorithm	-Compensated Errors: Amp., Phase -Suitable Application: Off-line, On-site, Online, Self-cal.	Amp., Phase	Rx
[35]	2015	BI	Phase center optimization	-Compensated Errors: Phase -Suitable Application: Off-line, On-site, Online	Phase	Rx
[11]	2016	BI	Impulse response difference	-Compensated Errors: Amp., Phase -Suitable Application: Off-line, On-site, Online, Self-cal.	Amp., Phase	Tx
[27]	2017	NF-FF-P	Solving linear equations	-Compensated Errors: MC -Suitable Application: Off-line, On-site	MC	Tx
[16]	2017	NF-FF-P	Active element pattern	-Compensated Errors: Amp., Phase, MC -Suitable Application: Off-line, On-site	Pattern	Tx
[33]	2018	MC	Graph coloring	-Compensated Errors: Amp., Phase, MC -Suitable Application: Off-line, On-site, Online, Self-cal.	MC	Rx/Tx
[36]	2018	BI	Code-Modulated Interferometry	-Compensated Errors: Amp., Phase -Suitable Application: Off-line, On-site, Self-cal.	Power	Rx/Tx
[1]	2019	PXP	Measured complex signals	-Compensated Errors: Amp., Phase -Suitable Application: Off-line, On-site	Amp., Phase	Tx
[2]	2019	BI	Measured complex signals	-Compensated Errors: Amp., Phase -Suitable Application: Off-line, On-site, Online, Self-cal.	Power	Rx
[14]	2019	PXP	MC measurement	-Compensated Errors: Amp., Phase, MC -Suitable Application: Off-line, On-site, Online, Self-cal.	MC	Rx/Tx
[22]	2020	NF-FF-P	MC measurement	-Compensated Errors: Amp., Phase, MC -Suitable Application: Off-line, On-site, Online, Self-cal.	MC	Rx/Tx
[26]	2020	NF-FF-P	Modified genetic algorithm	-Compensated Errors: Amp., Phase -Suitable Application: Off-line, Self-cal.	Power	Tx
[24]	2020	BI	Coupler integrated calibration	-Compensated Errors: Amp., Phase -Suitable Application: On-site, Self-cal.	Power	Rx
[28]	2021	NF-FF-P	Improved REV method	-Compensated Errors: Amp., Phase, MC -Suitable Application: Off-line	Power	Rx
[5]	2022	BI	Simultaneous perturbation	-Compensated Errors: Amp., Phase -Suitable Application: On-site, Online	Power	Rx
[13]	2022	BI	Closed-loop testing	-Compensated Errors: Amp., Phase, MC -Suitable Application: Off-line, Self-cal.	Amp., Phase, MC	Tx
[30]	2022	PXP	Compressed sensing	-Compensated Errors: Amp., Phase -Suitable Application: Off-line, On-site	Power	Tx
[29]	2023	NF-FF-P	Minimum vector-sum point	-Compensated Errors: Amp., Phase -Suitable Application: Off-line, Self-cal.	Power	Tx
[3]	2023	PXP	Code-division calibration	-Compensated Errors: Amp., Phase -Suitable Application: On-site, Online	Power	Rx
[18]	2023	PXP	Gaussian process model	-Compensated Errors: Amp., Phase, MC -Suitable Application: Off-line, On-site	Amp., Phase, MC	Rx
Proposed	2024	MC	Self MC measurement	-Compensated Errors: Amp., Phase, MC -Suitable Application: Off-line, On-site, Online, Self-cal.	MC	Tx

calibration method based on simultaneous perturbation is proposed, similar to [2], mutual couplings are ignored. There are extensive studies in the literature on the improvement of the mentioned calibration methods and their use in large-scale antenna arrays. Table 1 presents a chronological order of some of the prominent antenna array calibration work done over the last decade.

In this paper, we propose a novel built-in self-calibration method for transmit mode large-scale phased antenna arrays based on mutual coupling measurements. The proposed calibration method is capable of compensating gain/phase uncertainties, antenna element location errors and mutual coupling. The calibration procedure can be used in online calibration scheme as it will not cause any disruption to the system while it is operating. However, inter-element coupling measurements in the antenna array generally take a long time and may cause a delay in online calibration. These measurements are made automatically in advance and given as input to the system just once since the coupling between antennas does not depend on the pointing direction of the antenna array. In addition, mutual coupling measurements between an element and the elements in its second-order neighborhood are sufficient for accurate calibration. This leads significant reduction in measurement time and cost. Therefore, the proposed calibration method takes into account the couplings of certain number of neighboring elements.

In online procedure, the proposed calibration method combines the error feedback signal related to scan reflection coefficient (depends on the pointing direction) and the premeasured couplings to construct the array manifold. An error matrix is then estimated from the array manifold. The direct inverse of the error matrix is used for compensation matrix of the antenna weights. Direct inverse

matrix operations in hardware generally lead to inaccurate results because they involve division operations. Hence, a generalized inverse matrix approximation method is adopted, which reduces the matrix inverse operation to matrix sums and multiplications.

The main contributions of this study are summarized as follows:

1) The uncertainties as a function of scan reflection coefficient [16] for transmitting phased array antennas is described.
2) The proposed calibration method compensates for phase and amplitude changes caused by static and dynamic errors since automatic and continuous calibration is performed while the system is operating.
3) The proposed calibration method requires no additional testing reference signal. In addition, it is suitable for off-line, on-site and on-line calibration.
4) A generalized iterative inverse matrix approximation method [4] is adopted to improve the accuracy of estimation of the error compensation matrix in hardware.
5) The isolation problem related to the non-directional couplers mentioned in [13], is tackled by employing RF circulators for each antenna branch.

The remainder of this paper is organized as follows. In Section II, the theoretical modelling of phase and gain variations based on mutual coupling is explained. In Section III, the proposed calibration method is explained. In Section IV, numerical simulation results are presented to evaluate the performance of the proposed calibration method. In Section V, a simple experimental study is presented. Finally, Section VI concludes this paper.

Notations: Upper-case and lower-case boldface letters denote the matrices and vectors, respectively. $(.)^T$, $(.)^H$, $(.)^{-1}$, represent the transpose, conjugate transpose (Hermitian), and inversion, respectively. The $\odot$ operator represents the Hadamard product. The $\mathbf{I}_M$ is an identity matrix of size M.

II. THEORY

In this section, the basic concepts on phased array antennas, the main assumptions used through the proposed calibration method and error models are briefly explained. In this paper, the calibration of the phased antenna array operating in transmission mode is discussed and the contribution of the thermal effect is ignored.

A. ACTIVE ANTENNA ARRAY PATTERN

In applications of narrowband antenna arrays, radiating antennas are assumed to operate only in fundamental mode and it is considered that each element in the antenna array has almost the same pattern [16]. The antenna array pattern can be characterized by multiplying the array factor (AF) and the antenna element pattern. The array factor is the characterization of the antenna array in terms of complex phase shifts and amplitudes. The complete ideal active array pattern of the entire transmitting antenna array in the direction (θ_n, φ_n) which is defined in a $N_\theta \times N_\varphi$ angle grid, $E_a(\theta_n, \varphi_n)$, with M antennas can be expressed as follows:

$$E_a(\theta_n, \varphi_n) = E_e(\theta_n, \varphi_n) \underbrace{\sum_{m=1}^{M} V_m e^{jk\hat{\mathbf{r}}_n \vec{\mathbf{r}}_m}}_{AF} \tag{1}$$

where $E_e(\theta_n, \varphi_n)$ is the active element pattern defined in a $N_\theta \times N_\varphi$ angle grid, V_m is the excitation voltage of the m-th element being as $V_m = {V_m}^+ + {V_m}^-$, the phase of the m-th element is $\hat{\mathbf{r}}_n \vec{\mathbf{r}}_m = (x_m \sin\theta_n \cos\varphi_n + y_m \sin\theta_n \sin\varphi_n + z_m \cos\theta_n)$, $k = \frac{2\pi}{\lambda}$ and λ is the wavelength of the operating frequency and interelement spacing between two adjacent antenna element is $\frac{\lambda}{2}$ in both axis.

For a planar uniform array, the excitation voltage of the m-th element in the pointing direction $(\theta_0,\ \varphi_0)$ can be expressed as:

$${V_m}^+ = V_o e^{-j\frac{2\pi}{\lambda}(x_m \sin\theta_0 \cos\varphi_0 + y_m \sin\theta_0 \sin\varphi_0)} \tag{2}$$

where $V_o = 1$. Thus, the scan reflection of the one of those surrounding to the m-th element when all of the antenna elements are excited and properly phased to steer the array beam in the direction $(\theta_0,\ \varphi_0)$, can be expressed as:

$$\Gamma_m(\theta_0,\ \varphi_0) = \frac{{V_m}^-}{{V_m}^+} = e^{-jk\hat{\mathbf{r}}_0 \vec{\mathbf{r}}_m} \cdot \left(\mathbf{a_0}^T \mathbf{s}_{(m)}\right) \tag{3}$$

where $\mathbf{a_0}$ is the steering vector beings as $\mathbf{a_0} = [e^{jk\hat{\mathbf{r}}_0 \vec{\mathbf{r}}_1}, \ldots, e^{jk\hat{\mathbf{r}}_0 \vec{\mathbf{r}}_m}, \ldots, e^{jk\hat{\mathbf{r}}_0 \vec{\mathbf{r}}_M}]^T$ and $\mathbf{s}_{(m)}$ is a column of the scattering matrix of the planar antenna array up to K neighboring elements for each antenna element being as $\mathbf{s}_{(m)} = [S_{m1}, \ldots S_{mk}, \ldots S_{mK}]^T$.

The complete general planar array including reflection coefficients in the pointing direction with all elements excited can be written in more compact form as [16]:

$$\overline{E}_a(\theta_0,\ \varphi_0) = E_a(\theta_0,\ \varphi_0)\ \mathbf{a}^H(\mathbf{I}_M - \Gamma_\mathbf{0})\mathbf{v}^+ \tag{4}$$

where $\mathbf{v}^+$ is the vector of excitation voltages being as $\mathbf{v}^+ = [{V_1}^+, \ldots {V_m}^+, \ldots . {V_M}^+]^T$, $\Gamma_\mathbf{0}$ is a diagonal matrix of reflection coefficients and $\mathbf{I}_M$ is a $M \times M$ identity matrix.

As a next step, the active array pattern including modeling errors (reflection coefficients are also included) can be expressed as [31]:

$$\widetilde{E}_a(\theta_0,\ \varphi_0) = \mathbf{w}^H \widetilde{\boldsymbol{m}}(\theta_0,\ \varphi_0) E_a(\theta_0,\ \varphi_0) \tag{5}$$

where $\mathbf{w} \epsilon\ \mathbb{C}^{M\times 1}$ is the beamforming vector whose m-th term represents the complex beamforming weights of the m-th antenna element and $\widetilde{\boldsymbol{m}}(\theta_0,\ \varphi_0) \epsilon\ \mathbb{C}^{M\times 1}$ is the array manifold including mutual coupling effects, gain/phase errors and location errors of the antenna elements. The array manifold $\widetilde{\boldsymbol{m}}(\theta_0,\ \varphi_0)$ can be expressed as:

$$\widetilde{\boldsymbol{m}}(\theta_0,\ \varphi_0) = \mathbf{M}_e(\theta_0,\ \varphi_0)\mathbf{G}_{RF}\ (\boldsymbol{g}(\theta_0,\ \varphi_0) \odot \mathbf{a}(\theta_0,\ \varphi_0)) \tag{6}$$

where $\mathbf{G}_{RF} \epsilon\ \mathbb{C}^{M\times M}$ is the diagonal matrix, whose m-th diagonal element, $g_m^{RF} e^{-j\Psi_m^{RF}}$, represents the ideal

gain/phase coefficient of the RF chain of the m-th element, $\boldsymbol{g}(\theta_0,\ \varphi_0)\epsilon\ \mathbb{C}^{M\times 1}$ and $\mathbf{a}(\theta_0,\ \varphi_0)\epsilon\ \mathbb{C}^{M\times 1}$ are the vectors, whose m-th elements, $g_m e^{-j\Psi_m}$ and $e^{-j\delta_m}$ represent the ideal gain/phase coefficient and phase coefficients of the m-th element in the pointing direction $(\theta_0,\ \varphi_0)$, respectively, and $\mathbf{M}_e(\theta_0,\ \varphi_0)\epsilon\ \mathbb{C}^{M\times M}$ is the error matrix expressed as:

$$\mathbf{M}_e(\theta_0,\ \varphi_0) = \mathbf{C}(\Delta\mathbf{G}_{RF}\Delta\mathbf{G}(\theta_0,\ \varphi_0)\Delta\mathbf{A}(\theta_0,\ \varphi_0)) \quad (7)$$

where $\mathbf{C}\ \epsilon\ \mathbb{C}^{M\times M}$ is the mutual coupling matrix, $\Delta\mathbf{G}_{RF}\epsilon\ \mathbb{C}^{M\times M}$ is a diagonal matrix, whose m-th diagonal element, $\Delta g_m^{RF} e^{j\Delta\Psi_m^{RF}}$ represents the gain/phase uncertainty coefficient of the RF chain of the m-th element, $\Delta\mathbf{G}(\theta_0,\ \varphi_0)\epsilon\ \mathbb{C}^{M\times 1}$ and $\Delta\mathbf{A}(\theta_0,\ \varphi_0)\epsilon\ \mathbb{C}^{M\times 1}$ are the diagonal matrices, whose m-th diagonal elements, $\Delta g_m e^{j\Delta\Psi_m}$ and $e^{j\Delta\delta_m}$ represent the gain/phase uncertainty and phase uncertainty due to the location errors coefficients of the m-th element in the pointing direction $(\theta_0,\ \varphi_0)$, respectively.

In large-scale phased antenna array, the mutual coupling matrix, $\mathbf{C}$, can be constructed by taking account the only K neighbor elements of the m-th element where $K \ll M$. Phase and amplitude coupling coefficients of matrix $\mathbf{C}$ can be model based on the scan reflection coefficient, $C_{m,m}$, [16] and the coupling coefficients, $C_{m,k}$. The mutual coupling coefficients can be expressed as:

$$C_{m,m} = \frac{V_m^-}{V_m^+} = e^{jk(\hat{\mathbf{r}}_0-\hat{\mathbf{r}}_n)\vec{\mathbf{r}}_m}.\left(S_{mm} + \sum_{k=1}^{K} S_{mk} e^{-jk\hat{\mathbf{r}}_n\vec{\mathbf{r}}_k}\right) \quad (8)$$

$$C_{m,k} = \frac{V_k^-}{V_m^+} = S_{mk} e^{jk\hat{\mathbf{r}}_n\vec{\mathbf{r}}_m} e^{-jk\hat{\mathbf{r}}_n\vec{\mathbf{r}}_k} \quad (9)$$

where $\hat{\mathbf{r}}_n$ is the broadside unit vector, $\hat{\mathbf{r}}_k$ is the position vector of the k-th neighbor of the m-th element, S_{mk} is the magnitude of the scattering (coupling) coefficients of the m-th element and its k-th neighbor.

In line with (5)–(9), an array manifold matrix, $\widetilde{\mathbf{M}}(\theta_0,\ \varphi_0)$, which is later on defined as measurement matrix, in the pointing direction can be defined as:

$$\widetilde{\mathbf{M}}(\theta_0,\ \varphi_0) = \mathbf{M}_e(\theta_0,\ \varphi_0)\mathbf{G}_{RF}(\mathbf{G}(\theta_0,\ \varphi_0)\mathbf{A}(\theta_0,\ \varphi_0)) \quad (10)$$

where $\mathbf{G}(\theta_0,\ \varphi_0)\epsilon\ \mathbb{C}^{M\times M}$ and $\mathbf{A}(\theta_0,\ \varphi_0)\epsilon\ \mathbb{C}^{M\times M}$ are the diagonal matrices, whose m-th diagonal elements, $g_m e^{j\Psi_m}$ and $e^{j\delta_m}$ represent ideal gain/phase coefficient and phase coefficients of the m-th element in the pointing direction $(\theta_0,\ \varphi_0)$, respectively.

B. ACTIVE ELEMENT PATTERN

The characterization of a single active element pattern is useful the in characterization of an antenna array since, as stated in (1), the fully excited antenna array can be expressed in terms of the active element pattern and the array factor [31]. The active antenna element pattern of the m-th element of an antenna array can be expressed in terms of scan reflection coefficient and scattering coefficients in the pointing direction $(\theta_0,\ \varphi_0)$ as:

$$E_m(\theta_0,\ \varphi_0) = E_e(\theta_0,\ \varphi_0)e^{jk(\hat{\mathbf{r}}_0-\hat{\mathbf{r}}_n)\vec{\mathbf{r}}_m}.\left(1+\mathbf{s}_{(m)}\mathbf{d}_{(m)}\right) \quad (11)$$

where $E_m(\theta_0,\ \varphi_0)$ is the active element pattern of the m-th element defined a $N_\theta \times N_\varphi$ angle grid, $\mathbf{s}_{(m)}\epsilon\ \mathbb{C}^{1\times K}$ is the vector of magnitude of the scattering coefficients of the m-th element being as $\mathbf{s}_{(m)} = [S_{m1},\ldots,S_{mk}\ldots,S_{mK}]$ and $\mathbf{d}_{(m)}\epsilon\ \mathbb{C}^{1\times K}$ is the phase differences vector due to the location of K neighboring elements of the m-th element being as $\mathbf{d}_{(m)} = [e^{-jk\hat{\mathbf{r}}_0(\vec{\mathbf{r}}_1-\vec{\mathbf{r}}_m)},\ldots,e^{-jk\hat{\mathbf{r}}_0(\vec{\mathbf{r}}_k-\vec{\mathbf{r}}_m)},\ldots e^{-jk\hat{\mathbf{r}}_0(\vec{\mathbf{r}}_K-\vec{\mathbf{r}}_m)}]^T$.

In general, for large-scale antenna arrays, it is assumed that all the coupling coefficients are reciprocal as $S_{km} = S_{mk}$, however, this assumption may not always be valid as each element in the antenna array may have different excitation due to different error contributions. The gain/phase uncertainties that the active antenna element is exposed due to static and dynamic errors can be formulated in terms of mutual coupling. The radiated signal from the m-th antenna, which is imposed to gain/phase uncertainties, can be detected at a lower signal power level at neighboring antennas. Hence, by measuring the coupled signal from the neighboring antennas, gain and phase errors can be estimated.

The amplitude coefficients of the error matrix $\mathbf{M}_e(\theta_0,\ \varphi_0)$ are defined in terms of the element amplitude error (Δg_m), the amplitude error matrix of RF circuits (Δg_m^{RF}), and the mutual coupling. The amplitude error coefficients related with the m-th element and its k-th neighbor, $|g_{e(m,k)}|$, and due to the scan reflection, $|g_{e(m,m)}|$, can be expressed as [16]:

$$|g_{e(m,k)}| = \left|S_{mk}\Delta g_k^{RF}\Delta g_k\right| \quad (12)$$

$$|g_{e(m,m)}| = \left|S_{mm}\Delta g_m^{RF}\Delta g_m + \sum_{k=1}^{K} S_{mk}\Delta g_k^{RF}\Delta g_k\right| \quad (13)$$

The phase coefficients of the error matrix $\mathbf{M}_e(\theta_0,\ \varphi_0)$ are defined in terms of the phase uncertainty of the element due to the location error, phase uncertainty of the antenna element, phase uncertainty of RF circuit, and the mutual coupling. The amplitude error coefficients related with the m-th element and its k-th neighbor, $e^{j\Delta\Psi_{(m,k)}}$, and due to the scan reflection, $e^{j\Delta\Psi_{(m,m)}}$, can be expressed as [16]:

$$e^{j\Delta\Psi_{(m,k)}} = e^{j\Delta\delta_k}e^{j\Delta\Psi_k}e^{j\Delta\Psi_k^{RF}}e^{jk\hat{\mathbf{r}}_0(\vec{\mathbf{r}}_m-\vec{\mathbf{r}}_k)} \quad (14)$$

$$e^{j\Delta\Psi_{(m,m)}} = e^{j\Delta\delta_m}e^{j\Delta\Psi_m}e^{j\Delta\Psi_m^{RF}}\prod_{k=1}^{K} e^{j\Delta\Psi_{(m,k)}} \quad (15)$$

Then we can describe the entries of $\mathbf{M}_e(\theta_0,\ \varphi_0)$ as:

$$\mathbf{M}_e^{m,k} = |g_{e(m,k)}|e^{j\Delta\Psi_{(m,k)}} \quad (16)$$

$$\mathbf{M}_e^{m,m} = |g_{e(m,m)}|e^{j\Delta\Psi_{(m,m)}} \quad (17)$$

C. ERROR MATRIX ESTIMATION

The phased antenna array can be calibrated once the error matrix estimation performed. In order to estimate the error matrix $\mathbf{M}_e(\theta_0,\ \varphi_0)$ least-squares criteria can be

used [16], [37]. The cost function of the minimization problem can be expressed as:

$$\min_{\mathbf{M}_e(\theta_0,\ \varphi_0)} \left\| \widetilde{\mathbf{M}}(\theta_0,\ \varphi_0) - \mathbf{G}_{RF}(\mathbf{G}(\theta_0,\ \varphi_0)\mathbf{A}(\theta_0,\ \varphi_0)) \cdot \mathbf{M}_e(\theta_0,\ \varphi_0) \right\|_F^2 \tag{18}$$

Since the matrices $\mathbf{G}_{RF}$, $\mathbf{G}(\theta_0,\ \varphi_0)$ and $\mathbf{A}(\theta_0,\ \varphi_0)$ are priorly known, the unknown coefficients of the error matrix, $\mathbf{M}_e(\theta_0,\ \varphi_0)$, can be estimated as follows:

$$\mathbf{M}_e(\theta_0,\ \varphi_0) = \begin{pmatrix} (\mathbf{G}_{RF}(\mathbf{G}(\theta_0,\ \varphi_0)\mathbf{A}(\theta_0,\ \varphi_0)))^T \\ (\mathbf{G}_{RF}(\mathbf{G}(\theta_0,\ \varphi_0)\mathbf{A}(\theta_0,\ \varphi_0))) \end{pmatrix}^{-1} \cdot (\mathbf{G}_{RF}(\mathbf{G}(\theta_0, \varphi_0)\mathbf{A}(\theta_0,\ \varphi_0)))^T \widetilde{\mathbf{M}}(\theta_0, \varphi_0) \tag{19}$$

The gain/phase compensation of the complete phased antenna array, then, can be performed.

III. THE PROPOSED CALIBRATION METHOD

In this section, the flow of the proposed calibration method, the proposed online calibration system, calibration procedure and the required measurements, the adopted inverse matrix approximation method and the complexity of the proposed calibration method in terms of computational complexity and number of measurements are explained in detail.

A. FLOW OF THE PROPOSED CALIBRATION METHOD

The main idea of the calibration process is to acquire the coupled signals from the K neighbors of each antenna element to estimate the error matrix $\mathbf{M}_e(\theta, \varphi)$. The error matrix, then, can be used for compensating the gain/phase errors and the mutual coupling effects. The flow chart of the proposed procedure is given in Fig. 1.

The steps of the procedure are given as:

1) The theoretical ideal array pattern is pre-calculated according to pattern multiplication rule as in (1). The ideal weights of each element are determined according to the ideal gain/phase coefficients of $g_m^{RF} e^{-j\Psi_m^{RF}}$, $g_m e^{-j\Psi_m}$ and $e^{-j\delta_m}$. The pattern of single element is pre-measured and assumed to be identical for all elements. It should be noted the array geometry is known preliminary.
2) The mutual coupling coefficients of each antenna element from its K neighbors are measured. The calibration procedure is online; therefore, the mutual couplings should be pre-measured and saved in a look-up table.
3) The measurement signals are acquired from each antenna elements as $\widetilde{M}_{1,1}(\theta_0,\ \varphi_0), \ldots, \widetilde{M}_{M,M}(\theta_0,\ \varphi_0)$ in the pointing direction while the system is operating. It should be noted $\widetilde{M}_{m,m}(\theta_0,\ \varphi_0)$ is the scan reflection coefficient of the m-th element.
4) Construct the array manifold matrix, $\widetilde{\mathbf{M}}(\theta_0,\ \varphi_0)$, in the pointing direction by using the pre-measured mutual coupling coefficients and the measured scan reflection coefficients.
5) Estimate the error matrix, $\mathbf{M}_e(\theta_0,\ \varphi_0)$, using least squares solutions in (18). The inverse matrix in (18) can be pre-calculated since the coefficients of $\mathbf{G}_{RF}$, $\mathbf{G}(\theta_0,\ \varphi_0)$ and $\mathbf{A}(\theta_0,\ \varphi_0)$ are known.
6) An inverse matrix approximation method is used for calculating the inverse of the error matrix, $\mathbf{M}_e(\theta_0,\ \varphi_0)$ to obtain the compensation coefficients of the all elements.
7) The compensated array pattern in the pointing direction, $\widetilde{E}_a^c(\theta_0,\ \varphi_0)$, is calculated as:

$$\widetilde{E}_a^c(\theta_0,\ \varphi_0) = \mathbf{w}^H(\mathbf{M}_e(\theta_0,\ \varphi_0))^{-1}\widetilde{\mathbf{m}}(\theta_0,\ \varphi_0) \tag{20}$$

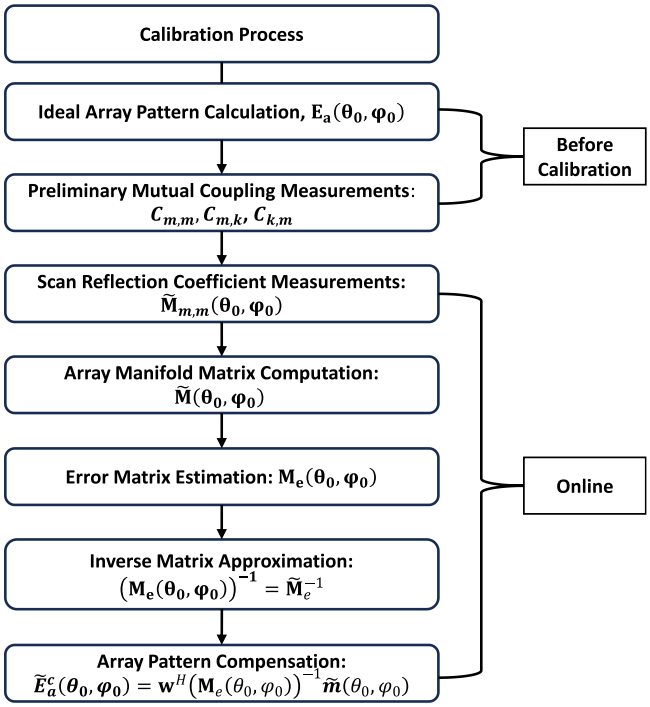

FIGURE 1. The flow chart of the proposed mutual coupling-based calibration method.

B. PROPOSED CALIBRATION SYSTEM

The topology of the proposed transmit array calibration system is depicted in Fig. 1. The calibration system consists of three main parts: 1) a transmit antenna array composed of *M* antenna elements, each connected to a circulator (CR) along with active and/or passive RF front end components such as band-pass filters (BF) and power amplifiers (PA) or power driver amplifiers (PDA), 2) a switching network (SW) composed of RF switches, down-converters baluns, 3) a RF system-on-chip (RF-SoC) FPGA for signal generation, base-band signal processing, switch controlling.

It should be noted that the proposed transmission array system calibration system has flexibility in RF component selection and circuitry. For example, if the frequency of the signal to be transmitted is lower than that of the DACs in the RF-SoC, there is no need to use up-converters in the RF beamformer chips or circuits. Thus, the structure is fully-digital beamforming in this case. However, can be easily

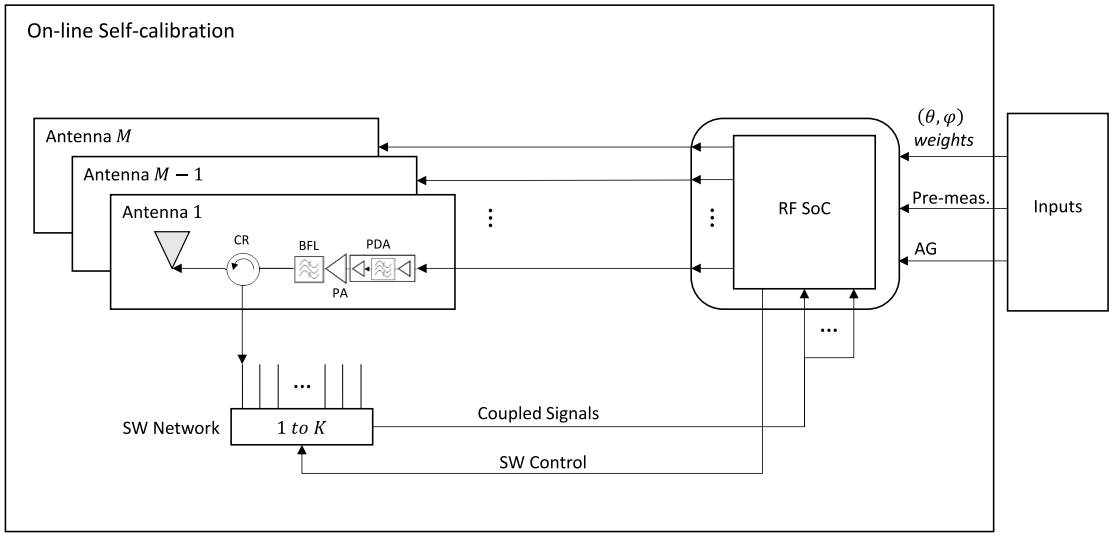

FIGURE 2. The proposed online large-scale antenna array self-calibration system.

extended to hybrid-beamforming applications by adding intermediate RF components (up-converters, RF beamformer chips or circuits, etc.) between the antenna array and the RF-SoC. The same is valid for the switching network, since the received signals from the circulators will be at the same frequency as the transmitting signal, therefore, there is no need to use down-converters for the frequencies lower than that of the ADCs. Moreover, if precision is not required for phase shifts, pin diodes or varactor diodes can be used instead of phase shifter chips for low frequencies to reduce system cost. Finally, in some cases, phase shifts can be performed in the baseband signal processing and in this case, phase shifters may not be needed. However, in order to realize the proposed on-line self-calibration method, circulators, and an RF-SoC are required to receive the feedback signals from the antenna elements in full digital architectures or antenna sub-arrays in hybrid architectures and process them in real-time to compensate for the described mutual coupling effects, gain/phase uncertainties, and location errors.

C. CALIBRATION PROCEDURE

The main idea of the calibration process with the transmit array calibration system defined above is to acquire signal samples from each antenna elements or each antenna sub-array with the aid of circulators to estimate the error matrix, $\mathbf{M}_e(\theta_0,\ \varphi_0)$, in the desired pointing direction with the signal processing in the RF-SoC, and then compensate the weight vector by taking the inverse of the error matrix.

Circulators provide high isolation at the cost of losing signal information of the RF chains connected to the antenna elements. However, measurements of the gain/phase uncertainties of the RF chains are not required since, as stated in (12)–(15), the gain/phase uncertainties of the m-th RF chain are included in total gain/phase deviation of the signal coupled to its k-th neighboring element and from the reflected signal from m-th element.

Assuming the single element pattern is known primarily, then, the $\mathbf{M}_e(\theta_0,\ \varphi_0)$ effects the AF and calibration is performed to improve the AF. The array manifold in the pointing direction $(\theta_0,\ \varphi_0)$ of the transmitting array including all the contributed errors only considering K neighboring element can be expressed as:

$$\widetilde{\mathbf{M}}(\theta_0,\ \varphi_0) = \begin{bmatrix} w_1 & 0 & \cdots & 0 \\ 0 & w_2 & \cdots & 0 \\ \vdots & \vdots & \ddots & \vdots \\ 0 & \cdots & 0 & w_M \end{bmatrix} \mathbf{M}_e(\theta_0,\ \varphi_0) \mathbf{G}_{RF}(\mathbf{G}(\theta_0,\ \varphi_0)\mathbf{A}(\theta_0,\ \varphi_0)) \tag{21}$$

$$\widetilde{\mathbf{M}}(\theta_0,\ \varphi_0) = \begin{bmatrix} \widetilde{M}_{1,1}, \ldots & \widetilde{M}_{1,k}, \ldots & \widetilde{M}_{1,K}, \ldots & 0 \\ \vdots \ldots & \vdots \ldots & \vdots \ldots & 0 \\ 0 & \widetilde{M}_{m,k}, \ldots & \widetilde{M}_{m,K} & \widetilde{M}_{M,M} \end{bmatrix} \tag{22}$$

Then, with a single measurement from all the active antennas while the system is operating, we can derive the following vector:

Finally, the proposed calibration procedure is based on the construction of the error matrix through automated measurements. The integrated circulators in the proposed transmission array calibration system are shown as in Fig. 3 allow measurements of only $\widetilde{M}_{m,m}$ and $\widetilde{M}_{m,k}$ but higher isolation yields higher precision.

The measurement procedure consists of two parts: first, to perform the off-line measurements of $\widetilde{M}_{m,k}$ and $\widetilde{M}_{k,m}$ coefficients that are independent of the pointing direction, are registered to a look-up-table and, second, the on-line measurements of $\widetilde{M}_{m,m}$ coefficients that depend on the pointing direction.

The coefficients, $\widetilde{M}_{m,m}$, are measured while the system is operating on the contrary the coefficients, $\widetilde{M}_{m,k}$ and $\widetilde{M}_{k,m}$ are premeasured automatically Fig. 3 depicts the measurements

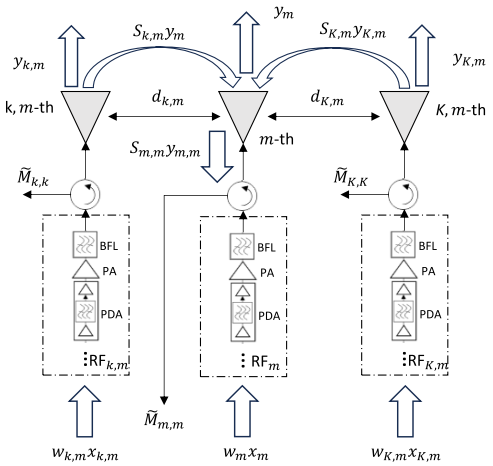

FIGURE 3. The measurements of the $\widetilde{M}_{m,m}$ coefficients related to scan reflection.

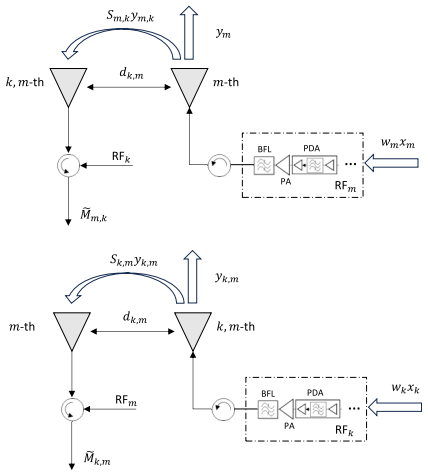

FIGURE 4. The measurements of the $\widetilde{M}_{m,k}$ and $\widetilde{M}_{k,m}$ coefficients related to inter-element coupling.

of $\widetilde{M}_{m,m}$ and Fig. 4 depicts the measurements of $\widetilde{M}_{m,k}$ and $\widetilde{M}_{k,m}$ (in case of unequal coupling). In Fig. 3 and Fig. 4 y denotes the radiated signal and x denotes the transmitted signal. The calibration system takes premeasured $\widetilde{M}_{m,k}$ and $\widetilde{M}_{k,m}$, coefficients, the array geometry (AG), antenna weights and the pointing direction as input.

D. INVERSE MATRIX APPROXIMATION

Direct inversion of matrices is unfavorable for hardware since direct inversion involves a division operator, which often leads to inaccurate results [4]. Therefore, many inverse matrix approximation methods have been proposed in the literature that degrades the inverse matrix operation to matrix multiplications and matrix sums. The most prominent inverse matrix approximation methods can be listed as Newton iteration method (NI), Chebyshev iteration method (CI) and successive over relaxation-based approximate matrix inversion method [38]. However, all of these methods require initial conditions and a Toeplitz or a symmetrical precondition matrix to guarantee the convergence [4].

In absence of reciprocity of mutual coupling between neighboring antennas, ($C_{mk} \neq C_{km}$), the convergence of these inverse matrix approximation methods is not guaranteed. Therefore, we adopted the inverse matrix approximation method in [4], which is globally convergent without needing any initial Toeplitz or symmetric matrix and preconditions. Then the error compensation matrix in the desired pointing direction, $\widetilde{\mathbf{M}}_e^{-1} \epsilon\ \mathbb{C}^{M\times M}$, can be approximated as:

$$\widetilde{\mathbf{M}}_e^{-1}(i+1) = \widetilde{\mathbf{M}}_e^{-1}(i) + \mathbf{X}\Big(\mathbf{M}_e^T - \mathbf{B}\widetilde{\mathbf{M}}_e^{-1}(i)\Big) \tag{24}$$

where i is the iteration number, $\mathbf{X} = (\mathbf{I}_M + (\mathbf{M}_e^T\mathbf{M}_e)^2)^{-1}$, $\mathbf{B} = (\mathbf{M}_e^T\mathbf{M}_e)^2$. The detailed formulation for the adopted inverse matrix approximation can be found in [4].

E. COMPLEXITY OF THE METHOD

The computational complexity of the proposed method lies in inverse matrix approximation method. According to [4], computational complexity for an antenna array with the number of antennas, M, is $O(8M^3 + 2M^2 + M)$ in terms of number of complex multiplications. If only K neighboring elements taking into account the computational complexity can be greatly reduced because of the zero entries in the error matrix. However, this discussion is not the subject of this paper. On the other hand, $2M(M-1)$ measurements are needed to extract the coupling coefficients if all the array elements are taken into account and there is no reciprocity between the elements. However, only $K(K-1)$ measurements are needed if only K neighboring elements are taken into account and there is reciprocity between the elements, then the number of measurements decrease significantly since $K \ll M$.

IV. SIMULATION RESULTS

In this section the simulation results are given to validate the effectiveness of the proposed calibration method. The

$$\begin{bmatrix} \widetilde{M}_{1,1}(\theta_0,\ \varphi_0) \\ \vdots \\ \widetilde{M}_{m,m}(\theta_0,\ \varphi_0) \\ \vdots \\ \widetilde{M}_{M,M}(\theta_0,\ \varphi_0) \end{bmatrix} = \begin{bmatrix} \mathbf{M}_e^{1,1} g_1^{RF} e^{-j\Psi_1^{RF}} g_1 e^{-j\Psi_1} e^{-j\delta_1} + \ldots + \mathbf{M}_e^{1,K} g_{1,K}^{RF} e^{-j\Psi_{1,K}^{RF}} g_{1,K} e^{-j\Psi_{1,K}} e^{-j\delta_{1,K}} \\ \vdots \\ \mathbf{M}_e^{m,m} g_m^{RF} e^{-j\Psi_m^{RF}} g_m e^{-j\Psi_m} e^{-j\delta_m} + \ldots + \mathbf{M}_e^{m,K} g_{m,K}^{RF} e^{-j\Psi_{m,K}^{RF}} g_{m,K} e^{-j\Psi_{m,K}} e^{-j\delta_{m,K}} \\ \vdots \\ \mathbf{M}_e^{M,M} g_M^{RF} e^{-j\Psi_M^{RF}} g_M e^{-j\Psi_M} e^{-j\delta_M} + \ldots + \mathbf{M}_e^{M,K} g_{M,K}^{RF} e^{-j\Psi_{M,K}^{RF}} g_{M,K} e^{-j\Psi_{M,K}} e^{-j\delta_{M,K}} \end{bmatrix} \tag{23}$$

TABLE 2. Standard uncertainties.

Parameter	Deviation Bounds
$\Delta\hat{x}_m$[mm]	$\pm$9.8157
$\Delta\hat{y}_m$[mm]	$\pm$9.8157
$\Delta\Psi_m$[°]	$\pm$1.7619
Δg_m[dB]	$\pm$0.5763
$\Delta\Psi_m^{RF}$[°]	$\pm$1.7619
Δg_m^{RF}[dB]	$\pm$0.5763

numerical examples are based on a planar uniform hexagonal array (UHA) formed by active antenna elements. Number of antenna elements are $M = 61$. Each antenna element has its own RF chain composed of active and passive RF components. Moreover, all elements follow the cosine squared antenna pattern. The inter element distances are $\frac{\lambda}{2}$ and $\sqrt{3}\frac{\lambda}{4}$ along x-axis and y-axis, respectively. The operating frequency is selected as 2.4 GHz.

Scattering parameters which represent the mutual coupling between antenna elements are calculated based on an assumption that 30 dB loss per wavelength, λ, on radiated signal power from one active antenna element. The corresponding coupled power is $\approx 3\%$ of the radiated signal power from one element to its neighboring element (-15 dB coupling). The scattering parameters are formed by multiplying magnitude coefficients, S_{mk}, and the phase coefficients, $e^{-jk\hat{\mathbf{r}}_0(\vec{\mathbf{r}}_k - \vec{\mathbf{r}}_m)}$ (location errors are included).

In simulations it is assumed no reciprocity between the elements ($C_{mk} \neq C_{km}$). The gain/phase deviations and location errors are modeled according to uncertainty analysis in [39] and are given in Table 2. The parameters are selected randomly with gamma distribution within the deviation bounds and the phase uncertainty, $\Delta\delta_m$, due to the location errors are related to shift in x-axis as $\Delta\widehat{x}_m$ and shift in y-axis as $\Delta\widehat{y}_m$.

Fig. 5 represents the UHA used in the simulations. In order to provide a better sight, the true locations and the erroneous locations of the antenna elements are given. In simulations, calibrations are performed according to the elements in the first-order neighborhood of the antenna elements, in the second-order neighborhood of the antenna elements and all other antenna elements in the array.

Fig. 6 represents the deviations in amplitude and phase of each element due to the uncertainties in antenna location and gain/phase errors for the simulations for broadside. Similar errors are computed for the other twos cases with $(\theta, \varphi) = (45°, 0°)$ and $(\theta, \varphi) = (30°, 60°)$.

Fig. 6 also shows that the total phase errors vary up to 8 degrees and gain errors vary up to 4.5 dB. High deviations are taken in account to demonstrate the performance of the method in the worst case.

Fig. 7 (a) shows the broadside $(\theta, \varphi) = (0°, 0°)$ pattern compensation. The comparison is performed taking into account calibration with the first-tier and the second-tier of antenna elements as well as full array elements using the inverse matrix approximation (IMA) method in [4]. Moreover, calibration using direct inversion (DI) for full

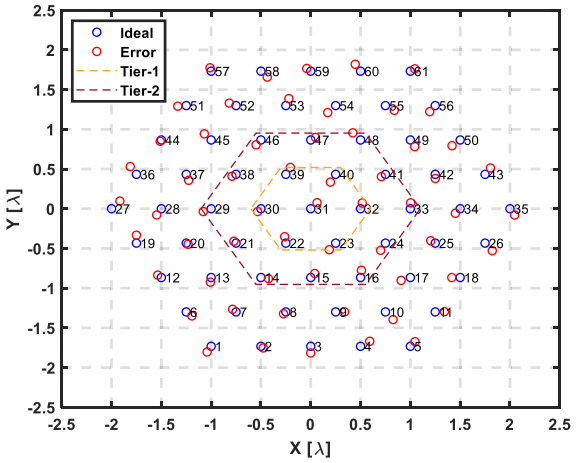

FIGURE 5. General uniform hexagonal antenna array with the true and the erroneous locations of the antenna elements.

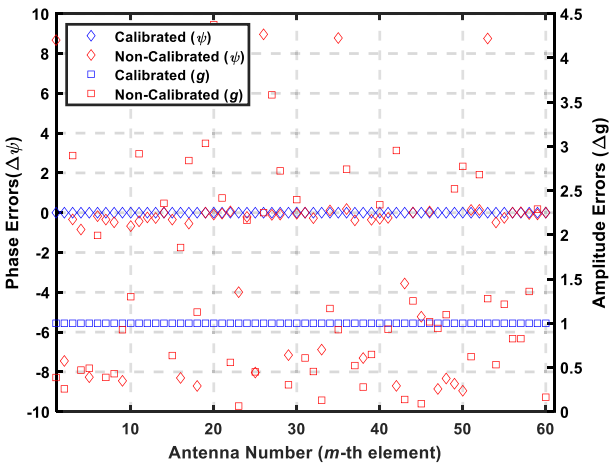

FIGURE 6. Element wise gain/phase deviations and calibrated gain/phase values for broadside using IMA Tier-2.

array elements is also included. Furthermore, ideal and not calibrated patterns are given for comparison with calibrated results.

After calibration, the pointing direction of compensated results are correct. In simulations, the maximum phase and locations errors are not too large to produce a phase center plane deviation. Besides, null depths vary as a function of the number of tiers used for mutual coupling effect meaning in a more accurate phase center location compensation. In broadside case, the high variations lead high side-lobe levels almost same level with pointing direction, also shallow nulls are occurred. In all compensation cases it results in significant improvements on reducing side-lobe levels and deeper nulls. As a remark, the deep nulls are important in interference mitigation. However, the results show that first-order tier compensation has the worst performance.

In Fig. 7 (b) same compensation performance can be observed for pointing direction in $(\theta, \varphi) = (45°, 0°)$. Comparisons show that the compensated patterns have at least 2.5 dB improvement in side-lobe level. Finally, Fig. 7

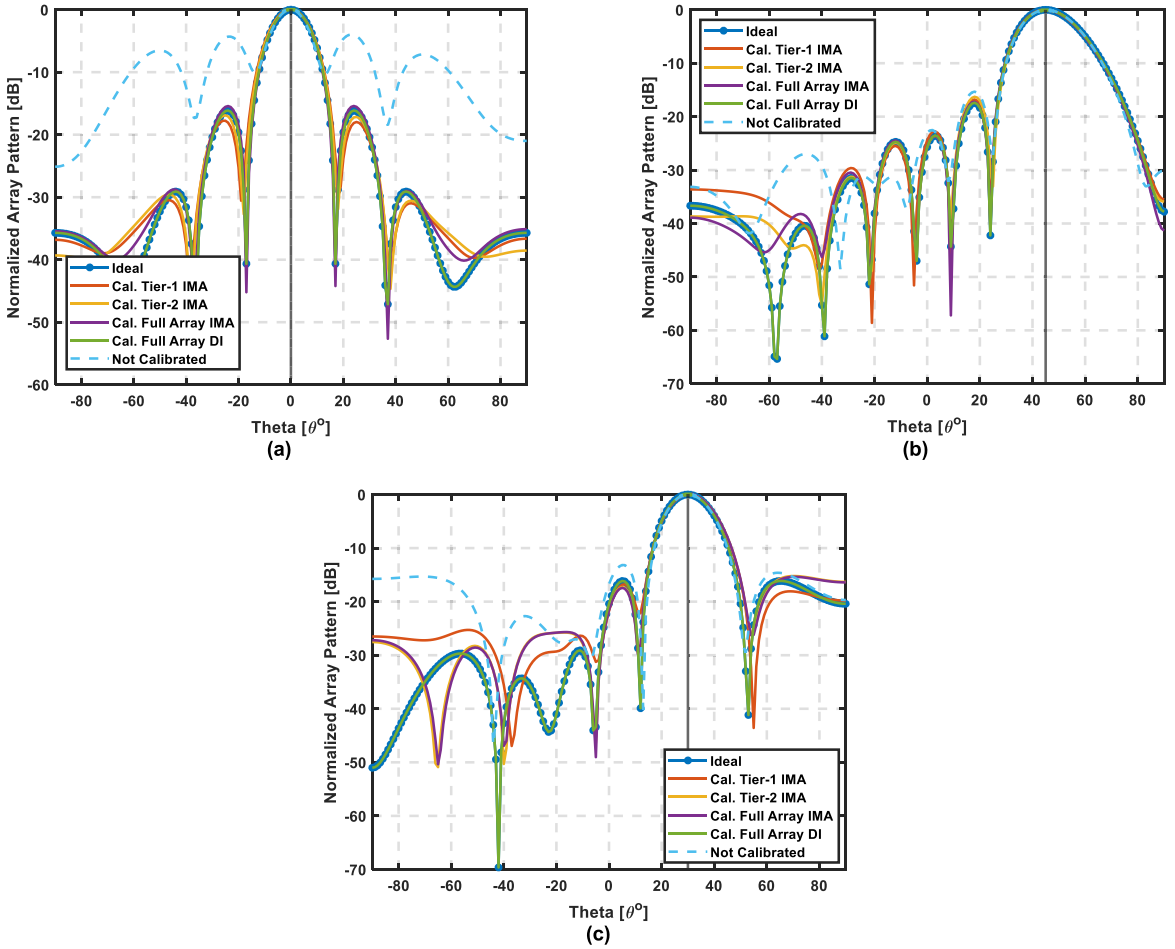

FIGURE 7. Comparison of ideal array pattern, array pattern after calibration with Tier-1 and Tier-2 using IMA, array pattern after calibration with full array elements using IMA, array pattern after calibration with full array elements using DI, and not calibrated array pattern in pointing directions: (a) $\theta = 0^\circ$ and $\varphi = 0^\circ$, (b) $\theta = 45^\circ$ and $\varphi = 0^\circ$, (c) $\theta = 30^\circ$ and $\varphi = 60^\circ$.

(c) represents the results for $(\theta, \varphi) = (30^\circ, 60^\circ)$ and it can be concluded that the compensation can be performed in two-dimensional plane. Finally, in all three cases the compensation is performed on the array factor and the antenna patterns are identical for all antenna elements.

As final remarks, 1) compensation performances of full-array inverse matrix approximation method and direct inversion are almost identical, 2) to reduce the side-lobe levels, the mutual coupling of more neighboring antenna elements are needed to be taken into account, 3) compensation with only first-order or second-order tiers result in reduced precision in calibration, however, more practical for large-scale antenna arrays since only K measurements are needed instead of M measurements where $K \ll M$. It should be noted K or M measurements are needed if reciprocity is assumed between elements, otherwise, $2K$ or $2M$ measurements are needed.

V. EXPERIMENTAL STUDY

In this section we present an experimental study to validate our proposed calibration method. For reduction of complexity and general implementation without lack of validity we conducted a simple experimental study using a linear four-element dipole antenna array ($M = 4$). Fig. 9 and Fig. 10 show the experimental set-up and its main components. The components of the proposed experimental setup can be listed as follows:

- Antenna array in two pairs to produce differences in gain and phase, for a total of 4 dipole antennas,
- RF cables,
- An on-the-shelf circulator,
- A RFSoC 4x2 board, a high-performance computing system optimized for sampling and generating signals at up to 9.85GSPS. Based on AMD-Xilinx ZYNQ Ultrascale+ Gen3 RFSoC device, the board offers four high-speed ADC ports (white blocks, tile 224 and 226), two high-speed DAC ports (white blocks, tile 228 and 230), 8GBytes of fast DDR4 memory, and a QSFP28 port for high-speed data offload. The RFSoC board is ideally suited to serve as a powerful and highly configurable software defined radio (SDR) system. The AMD-Xilinx ZYNQ UltraScale+ device includes a quad-core ARM Cortex-A53, a dual-core ARM Cortex

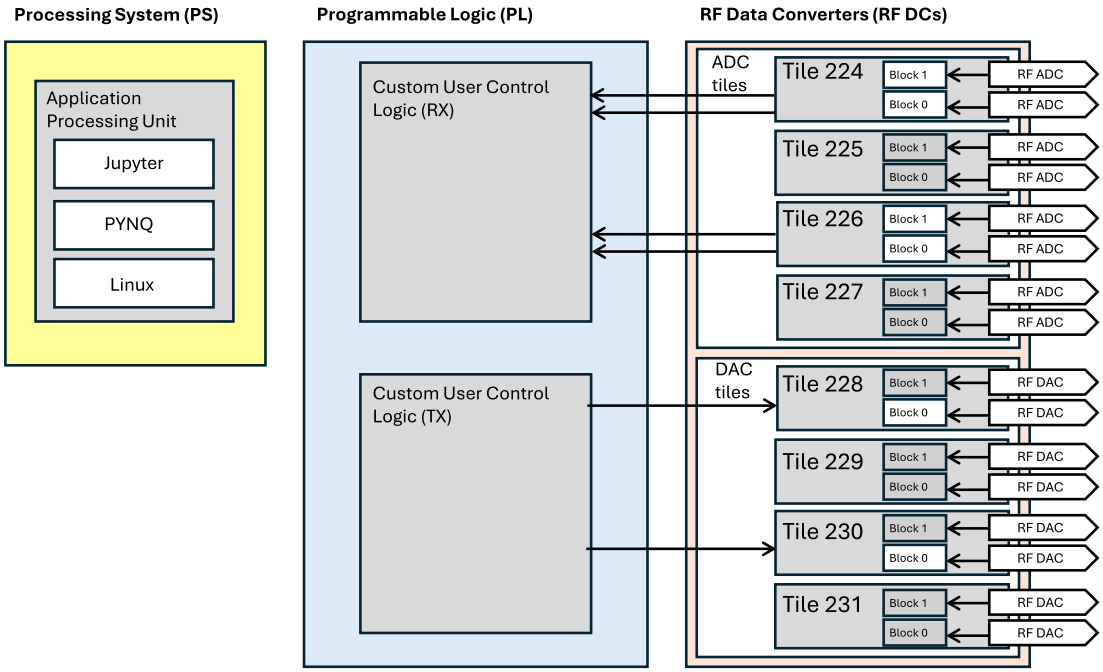

FIGURE 8. Processing system description for the FPGA unit for the measurements.

R5F, monolithic direct RF-sampling ADCs and DACs, and several other high-performance cores to assist with acquiring and processing high speed data.

- The RFSoC board works with all AMD-Xilinx Vitis/Vivado tools and the PYNQ open-source framework.
- The RFSoC 4x2 board is centered around the ZYNQ XCZU48DR UltraScale+ RFSoC device from AMD-Xilinx, and the most critical features are implemented in the AMD-Xilinx device. The XCZUDR48 includes:

Processing System:

- A 64-bit quad-core ARM Cortex-A53 and a 32-bit dual-core ARM Cortex-R5F
- An ARM Mali-400 based GPU and NEON advanced SIMD media processing engine

Programmable Logic

- Large Programmable logic array with 930K logic cells and 4.2K DSP slices
- IEEE 802.3 compliant 100G Ethernet

RF System:

- 8 14-bit RF ADCs with 5.0GSPS max sample rate
- 8 14-bit RF DACs with 9.85GSPS max sample rate
- 8 SD-FEC IP blocks

All elements works at the frequency used for the tests (2.4 GHz). It should be noted that the mutual coupling measurements were made using the FGPA board, but the calibration was done with post-processing using MATLAB on the raw data obtained.

Fig. 8 shows the components used in the test. In the Processing System (PS) an application has been implemented to obtain the data of the synchronized signals on the Jupyter notebooks, using the PYNQ framework on Linux. In the

FIGURE 9. Rack with RFSoC and experimental antenna elements for coupling coefficient measurements C_{mk} and C_{km}.

Programmable Logic (PL) two different chains have been implemented, one for signal transmission and the other for reception.

Finally, the RF Data Converters used all the modules available on the board (4 ADCs and 2 DACs), marked in white in the Fig. 8, synchronized using the Multi Tile Synchronization algorithm.

In the proposed experimental system, the RF beamformer chip(s) or circuit(s) and switching network proposed in Fig. 2 are excluded. Note that BF chips can be used for hybrid architecture implementation while circuits only include RF chains. Additionally, since the RF-SoC used has only 2 DACs, in the baseband, no phase shift is

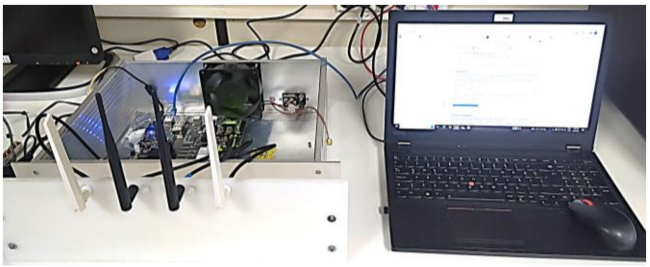

FIGURE 10. Measurement setup including computer for measurement acquisition for coupling coefficient measurements C_{mk} and C_{km}.

applied to the generated signal. Therefore, experimental work is carried out only on the broadside. The relationship between source direction and mutual coupling is described above in the scan coefficient of the mutual coupling model used. However, as per Fig. 7, the mutual coupling effects, gain/phase uncertainties, and location errors on the antenna array pattern at the broadside is the most significant case.

The details of the experimental procedure are given as below:

1) In the measurements, first premeasurements of the coupling coefficients are conducted. Each element in the antenna array is respectively in transmitter mode and connected to the DAC-A connector on the RF-SoC (which can also be connected to DAC-B). Then, the transmitter antenna is fed with a sinusoidal signal of 2.4 GHz frequency and 0 dBm power, respectively, and the couplings (C_{km}) between the antennas are measured. Then, 3 antennas are connected to the DAC-A port to operate in transmitter mode with an on-the-self power divider, and C_{mk} coefficients are measured one-by-one. In order to compensate for the losses in the power divider, the DAC-A port was fed with a sinusoidal signal at 2.4 GHz frequency and 7 dBm power. Since the phase shifts and losses are different in the cables to which the antennas are connected, non-reciprocity occurs as, $C_{mk} \neq C_{km}$. Additionally, there are slightly different phase shifts and losses between ports in the power divider.
2) In the second part, the measurements of the scan reflection coefficients, C_{mm}, are conducted. In this regard, all antennas are operated in transmitting mode. For this, the power divider is connected to the DAC-A port on the RF-SoC, and the DAC-A port is fed with a sinusoidal signal at 2.4 GHz frequency and 10 dBm power. Then, a circulator is connected sequentially between each antenna and the power divider outputs, and the feedback signals are measured one-by-one by connecting the third port of the circulator to the ADC-A port on the RF-SoC.
3) As a third step, two array manifold matrices including mutual coupling, gain/phase uncertainties and location errors, are created for comparison, one for calibration with the first-order tiers and one for calibration the full array elements. Since the relationship between mutual coupling and phase changes due to gain/phase uncertainties and position errors has been explained previously, the measured C_{mk}, C_{mk} and C_{mm} coefficients are the entries of the array manifold matrix $\widetilde{\mathbf{M}}(\theta_0,\ \varphi_0)$. The two array matrices (pointing to broadside) are given respectively as:

$$\widetilde{\mathbf{M}}_1 = \begin{bmatrix} C_{11} & C_{12} & 0 & 0 \\ C_{21} & C_{22} & C_{23} & 0 \\ 0 & C_{32} & C_{33} & C_{34} \\ 0 & 0 & C_{43} & C_{44} \end{bmatrix} \tag{25}$$

$$\widetilde{\mathbf{M}}_2 = \begin{bmatrix} C_{11} & C_{12} & C_{13} & 0 \\ C_{21} & C_{22} & C_{23} & C_{24} \\ C_{31} & C_{32} & C_{33} & C_{34} \\ 0 & C_{42} & C_{43} & C_{44} \end{bmatrix} \tag{26}$$

$$\widetilde{\mathbf{M}}_F = \begin{bmatrix} C_{11} & C_{12} & C_{13} & C_{14} \\ C_{21} & C_{22} & C_{23} & C_{24} \\ C_{31} & C_{32} & C_{33} & C_{34} \\ C_{41} & C_{42} & C_{43} & C_{44} \end{bmatrix} \tag{27}$$

4) Once the first-order tier, $\widetilde{\mathbf{M}}_1$, the second-order tier $\widetilde{\mathbf{M}}_2$ and full array, $\widetilde{\mathbf{M}}_F$, manifolds are created, then, the coefficients of the error matrices are estimated according to (15)–(16).
5) In the last step, the inverse matrix approximation method is applied to compensate the error matrices.

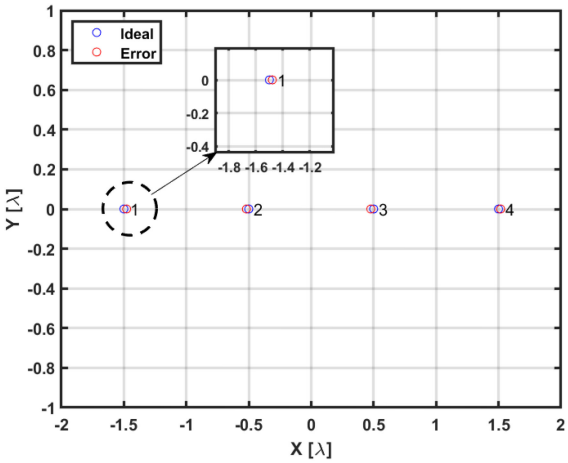

FIGURE 11. General uniform 4-element linear antenna array with the true and the erroneous locations of the antenna elements.

Fig. 11 represents the 4-element uniform linear array consisting of dipole antenna elements which are used in the experimental study. In order to provide a better sight, the true locations and the coarse erroneous locations of the antenna elements are given. The separation between antenna elements is half wavelength for 2.4 GHz. The coarse erroneous locations of the antenna elements are extracted by using the equations (13)–(14) once we measure all the phase uncertainties of cables, antenna elements, circulators and so on in the experimental setup. It should be noted this step

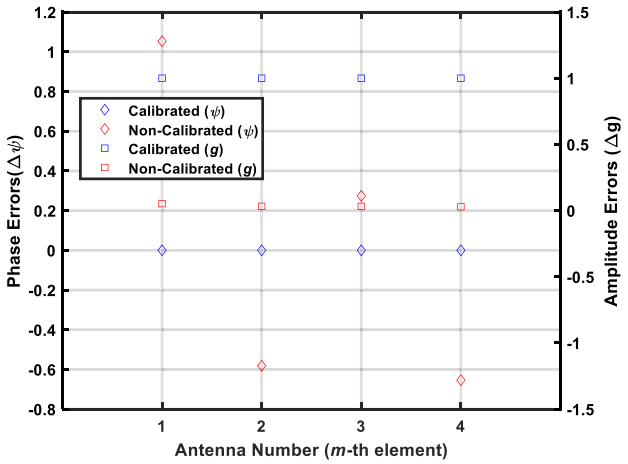

FIGURE 12. Element wise gain/phase deviations and calibrated gain/phase values for broadside using IMA Tier-2.

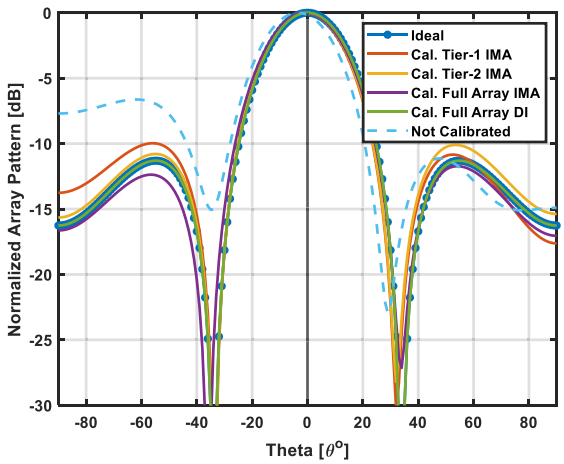

FIGURE 13. Comparison of ideal array pattern, after calibration with: Tier-1 and Tier-2 using IMA, full array elements using IMA, full array elements using DI, and not calibrated array pattern, all in the pointing direction: $\theta = 0^\circ$.

does not effect nor is related with the calibration procedure, however, Fig. 11 is given to show that after measuring the phase errors of the elements in the system, the coarse location of the antenna elements can be estimated if required.

Fig. 12 represents the deviations in amplitude and phase of each element due to the uncertainties in antenna location and gain/phase errors from the measurement results for broadside. In addition, element wise calibrated gain/phase values for broadside using IMA Tier-2 is given in Fig. 12. It can be observed that the total phase errors vary up to 1.1 degrees and gain errors vary up to 0.25 dB. In the measurements it can be seen that the amplitude and phase variations are much lower than simulations.

Fig. 13 shows the broadside $(\theta, \varphi) = (0^\circ, 0^\circ)$ pattern compensation. The comparison between calibration with the first-tier and the second-tier of antenna elements as well as full array elements using the inverse matrix approximation (IMA) method in [4], calibration using direct inversion (DI) for full array elements, and ideal and not calibrated patterns is given just like in the simulation results. It can be seen that, in practice, the elements in the system have different amplitude and phase deviations resulting in unequal mutual couplings. In addition, since 2.4 GHz is the Wi-Fi frequency, other radiating components in the environment also interacts with the experimental setup in either constructive or destructive way. Moreover, even the amplitude and phase deviations are lower than those in simulations the unequal patterns of the individual antennas cause phase center plane shift, thus, shift in the pointing direction of uncalibrated array can be observed in Fig. 13. However, since the calibration is done on array factor, with calibrating each element according to estimated errors, the pointing direction can be also corrected.

The calibration results in Fig. 13 for the broadside demonstrates that the compensation of amplitudes and phases, as well as, phase center plane shift are correct. It can be seen that null depths vary as a function of the number of tiers used for mutual coupling effect meaning in a more accurate phase center location compensation as demonstrated in simulation results. In Fig. 13, it can be seen that with the proposed method at least 3 dB reduction in the left-side side-lobe level and also the side-lobe levels are equalized. Moreover, the shallow nulls are improved and most important of all the shift in pointing direction is compensated.

VI. CONCLUSION

In this paper we proposed a mutual coupling-based self-calibration method which is suitable for off-line, on-site and online calibration schemes. The calibration method capable of compensating mutual coupling effect, and gain and phase errors, as well as, phase center plane shift. The method is based on the estimation of the phase center and suitable for any array topology. The compensation weights were derived from the phase center obtained with least-squares solutions, and the expansion of the active element pattern for active antenna arrays. However, the compensation matrix was derived with an inverse matrix approximation method.

The theory for the analytical validation of the proposed method has been addressed, and the effect of gain/phase uncertainties, location errors and mutual coupling on phase center has been demonstrated. The effectiveness of the proposed method is validated by simulation results under worst conditions. The simulation results show that the compensated patterns have at least 2.5 dB improvement in side-lobe levels and have deeper nulls.

Furthermore, a four-element simple experimental system is set-up to verify the effectiveness of the proposed method in practice. An RF-SoC FPGA was used to measure the coupling between antenna elements and the measured raw data was post-processed. It has been seen that unequal mutual couplings and antenna patterns lead in unequal side-lobe levels and phase center plane shift in practice. The experimental study shows that the proposed method at least 3 dB improvement in side-lobe levels and have deeper nulls, as well as, has the capability of compensating phase center plane shift.

REFERENCES

[1] F. Zhang, W. Fan, Z. Wang, Y. Zhang, and G. F. Pedersen, "Improved over-the-air phased array calibration based on measured complex array signals," *IEEE Antennas Wireless. Propag. Lett.*, vol. 18, no. 6, pp. 1174–1178, Jun. 2019, doi: 10.1109/LAWP.2019.2911725.

[2] D.-C. Kim, S.-J. Park, T.-W. Kim, L. Minz, and S.-O. Park, "Fully digital beamforming receiver with a real-time calibration for 5G mobile communication," *IEEE Trans. Antennas Propag.*, vol. 67, no. 6, pp. 3809–3819, Jun. 2019, doi: 10.1109/TAP.2019.2902712.

[3] Y. Lin, C. Hu, Z. Shi, B. Liang, and J. Li, "Low-complexity online calibration for large-scale multi-beam antennas," *Electronics*, vol. 12, no. 7, p. 1690, Apr. 2023, doi: 10.3390/electronics12071690.

[4] A. E. Zorkun, M. A. Salas-Natera, and R. M. Rodriguez-Osorio, "Improved iterative inverse matrix approximation algorithm for zero forcing precoding in large antenna arrays," *IEEE Access*, vol. 10, pp. 100964–100975, 2022, doi: 10.1109/ACCESS.2022.3208155.

[5] H. Xing et al., "Antenna array calibration methods based on simultaneous perturbation," *IET Microw. Antenna Propag.*, vol. 16, no. 14, pp. 898–909, Nov. 2022, doi: 10.1049/mia2.12304.

[6] Y. Ji, J. Ø. Nielsen, and W. Fan, "A simultaneous wideband calibration for digital beamforming arrays at short distances [measurements corner]," *IEEE Antennas Propag. Mag.*, vol. 63, no. 3, pp. 102–111, Jun. 2021, doi: 10.1109/MAP.2021.3069244.

[7] G. He, X. Gao, and R. Zhang, "Impact analysis and calibration methods of excitation errors for phased array antennas," *IEEE Access*, vol. 9, pp. 59010–59026, 2021, doi: 10.1109/ACCESS.2021.3073222.

[8] S. Daneshmand, N. Sokhandan, M. Zaeri-Amirani, and G. Lachapelle, "Precise calibration of a GNSS antenna array for adaptive beamforming applications," *Sensors*, vol. 14, no. 6, pp. 9669–9691, Jun. 2014, doi: 10.3390/s140609669.

[9] J. Pérez Santacruz et al., "Outdoor mm-Wave 5G/6G transmission with adaptive analog beamforming and IFoF fronthaul," *Sci. Rep.*, vol. 13, no. 1, Aug. 2023, Art. no. 13945, doi: 10.1038/s41598-023-40112-w.

[10] P. B. Anantharamu, D. Borio, and G. Lachapelle, "Self-contained antenna array calibration using GNSS signals," *Navigation*, vol. 59, no. 3, pp. 209–220, 2012, doi: 10.1002/navi.16.

[11] K. Kim, H. Yang, J. Jang, T. Sun, S. Choi, and J. Jung, "Online calibration for LTE-based antenna array system," *Int. J. Antennas Propag.*, vol. 2016, pp. 1–10, Jan. 2016, doi: 10.1155/2016/2645870.

[12] D. H. Rogstad, "The SUMPLE algorithm for aligning arrays of receiving radio antennas: Coherence achieved with less hardware and lower combining loss," Jet Propulsion Lab., California Inst. Technol., Pasadena, CA, USA, IPN Progress Rep. 42-162, 2005.

[13] B. M. Fabiani et al., "Closed-loop controlled microwave beamformer," *Int. J. RF Microw. Comput.-Aided Eng.*, vol. 32, no. 3, 2022, Art. no. e23020, doi: 10.1002/mmce.23020.

[14] A. Nafe, K. Kibaroglu, M. Sayginer, and G. M. Rebeiz, "An in-situ self-test and self-calibration technique utilizing antenna mutual coupling for 5G multi-beam TRX phased arrays," in *Proc. IEEE MTT-S Int. Microw. Symp. (IMS)*, Jun. 2019, pp. 1229–1232, doi: 10.1109/MWSYM.2019.8701072.

[15] I. Seker, "Calibration methods for phased array radars," in *Proc. Radar Sens. Technol.*, 2013, Art. no. 87140W, doi: 10.1117/12.2015694.

[16] M. A. Salas-Natera, R. M. Rodriguez-Osorio, L. de Haro Ariet, and M. Sierra-Perez, "Novel reception and transmission calibration technique for active antenna array based on phase center estimation," *IEEE Trans. Antennas Propag.*, vol. 65, no. 10, pp. 5511–5522, Oct. 2017, doi: 10.1109/TAP.2017.2738067.

[17] R. Long, J. Ouyang, F. Yang, W. Han, and L. Zhou, "Fast amplitude-only measurement method for phased array calibration," *IEEE Trans. Antennas Propag.*, vol. 65, no. 4, pp. 1815–1822, Apr. 2017, doi: 10.1109/TAP.2016.2629467.

[18] S. S. Tambovskiy, G. Fodor, and H. M. Tullberg, "Antenna array calibration via Gaussian process models," Jan. 31, 2023, *arXiv:2301.06582*.

[19] A. Stark, B. Rohrdantz, U. Johannsen, and A. F. Jacob, "In-situ probes for patch antenna array calibration," *Int. J. Microw. Wireless Technol.*, vol. 3, no. 3, pp. 273–280, Jun. 2011, doi: 10.1017/S1759078711000316.

[20] C. Fulton et al., "Cylindrical polarimetric phased array radar: Beamforming and calibration for weather applications," *IEEE Trans. Geosci. Remote Sens.*, vol. 55, no. 5, pp. 2827–2841, May 2017, doi: 10.1109/TGRS.2017.2655023.

[21] J. Lujan, C. J. Fulton, M. Yeary, E. A. Langley, S. McCormick, and A. Hedden, "Phased array radar initial alignment algorithm using mutual coupling: An iterative approach," in *Proc. Radar Sens. Technol.*, Apr. 2020, Art. no. 1140811, doi: 10.1117/12.2562963.

[22] R. M. Lebron, P.-S. Tsai, J. M. Emmett, C. Fulton, and J. L. Salazar-Cerreno, "Validation and testing of initial and in-situ mutual coupling-based calibration of a dual-polarized active phased array antenna," *IEEE Access*, vol. 8, pp. 78315–78329, 2020, doi: 10.1109/ACCESS.2020.2983523.

[23] O. Inac, D. Shin, and G. M. Rebeiz, "A phased array RFIC with built-in self-test capabilities," *IEEE Trans. Microw. Theory Techn.*, vol. 60, no. 1, pp. 139–148, Jan. 2012, doi: 10.1109/TMTT.2011.2170704.

[24] S.-C. Chae, H.-W. Jo, J.-I. Oh, G. Kim, and J.-W. Yu, "Coupler integrated microstrip patch linear phased array for self-calibration," *IEEE Antennas Wireless Propag. Lett.*, vol. 19, no. 9, pp. 1615–1619, Sep. 2020, doi: 10.1109/LAWP.2020.3011862.

[25] A. Dreher, N. Niklasch, F. Klefenz, and A. Schroth, "Antenna and receiver system with digital beamforming for satellite navigation and communications," *IEEE Trans. Microw. Theory Techn.*, vol. 51, no. 7, pp. 1815–1821, Jul. 2003, doi: 10.1109/TMTT.2003.814309.

[26] C.-N. Hu, P. Lo, C.-P. Ho, and D.-C. Chang, "Automatic calibration using a modified genetic algorithm for millimeter-wave antenna modules in MIMO systems," *Int. J. Antennas Propag.*, vol. 2020, Jun. 2020, Art. no. e4286026, doi: 10.1155/2020/4286026.

[27] R. Long, J. Ouyang, F. Yang, W. Han, and L. Zhou, "Multi-element phased array calibration method by solving linear equations," *IEEE Trans. Antennas Propag.*, vol. 65, no. 6, pp. 2931–2939, Jun. 2017, doi: 10.1109/TAP.2017.2694767.

[28] H.-J. Yoon and B.-W. Min, "Improved rotating-element electric-field vector method for fast far-field phased array calibration," *IEEE Trans. Antennas Propag.*, vol. 69, no. 11, pp. 8021–8026, Nov. 2021, doi: 10.1109/TAP.2021.3083796.

[29] S. Kim, H.-J. Dong, J.-W. Yu, and H. L. Lee, "Phased array calibration system with high accuracy and low complexity," *Alexandria Eng. J.*, vol. 69, pp. 759–770, Apr. 2023, doi: 10.1016/j.aej.2023.02.026.

[30] A. O. Fadamiro and F. Lin, "A compressed sensing approach for antenna array calibration," *Telkomnika*, vol. 20, no. 4, p. 892, Aug. 2022, doi: 10.12928/telkomnika.v20i4.23767.

[31] M. A. Salas-Natera, R. M. Rodriguez-Osorio, and L. de Haro, "Procedure for measurement, characterization, and calibration of active antenna arrays," *IEEE Trans. Instrum. Meas.*, vol. 62, no. 2, pp. 377–391, Feb. 2013, doi: 10.1109/TIM.2012.2217662.

[32] Y. Dong, S. Dong, Y. Wang, and L. Gong, "Calibration method of retrodirective antenna array for microwave power transmission," in *Proc. IEEE Wireless Power Transf. (WPT)*, Perugia, Italy, May 2013, pp. 41–43. doi: 10.1109/WPT.2013.6556876.

[33] L. Yang, R. Dang, M. Li, K. Zhao, C. Song, and Z. Xu, "A fast calibration method for phased arrays by using the graph coloring theory," *Sensors*, vol. 18, no. 12, p. 4315, Dec. 2018, doi: 10.3390/s18124315.

[34] Q. Huang, H. Zhou, J. Bao, and X. Shi, "Mutual coupling calibration for microstrip antenna arrays via element pattern reconstruction method," *IEEE Antennas Wireless Propag. Lett.*, vol. 13, pp. 51–54, 2014, doi: 10.1109/LAWP.2013.2296073.

[35] K. Hu, X. Zhang, J. Shi, and S. Wei, "A novel antenna phase center estimation method for synthetic aperture radar," in *Proc. IEEE Radar Conf. (RadarCon)*, May 2015, pp. 1340–1344. doi: 10.1109/RADAR.2015.7131203.

[36] K. Greene, V. Chauhan, and B. Floyd, "Built-in test of phased arrays using code-modulated interferometry," *IEEE Trans. Microw. Theory Techn.*, vol. 66, no. 5, pp. 2463–2479, May 2018, doi: 10.1109/TMTT.2017.2784373.

[37] M. Mowlér, B. Lindmark, E. G. Larsson, and B. Ottersten, "Joint estimation of mutual coupling, element factor, and phase center in antenna arrays," *J. Wireless Commun. Netw.*, vol. 2007, no. 1, Dec. 2007, Art. no. 30684, doi: 10.1155/2007/30684.

[38] F. Rosario, F. A. Monteiro, and A. Rodrigues, "Fast matrix inversion updates for massive MIMO detection and precoding," *IEEE Signal Process. Lett.*, vol. 23, no. 1, pp. 75–79, Jan. 2016, doi: 10.1109/LSP.2015.2500682.

[39] M. A. Salas-Natera and Rodrez-Osorio, "Analytical evaluation of uncertainty on active antenna arrays," *IEEE Trans. Aerosp. Electron. Syst.*, vol. 48, no. 3, pp. 1903–1913, Jul. 2012, doi: 10.1109/TAES.2012.6237569.

ARAL ERTUG ZORKUN received the B.S. degree in electrical and electronics engineering from Sabancı University in 2013, and the M.S. degree in electrical and electronics engineering from the TOBB University of Economics and Technology in 2018. He is currently pursuing the Ph.D. degree with the Universidad Politécnica de Madrid, Madrid, Spain.

He is currently with the Radiation Group, Universidad Politécnica de Madrid.

MIGUEL A. SALAS-NATERA received the master's degree in space technologies and the Ph.D. degree in technologies and communications systems from the Universidad Politécnica de Madrid (UPM) in 2011 and 2011, respectively.

He is an Electrical Engineer of Telecommunications. One year later, he was the Technical Director of Antenna System Solutions Company (spin-off of the UPM) for two years. Then, he has made Postdoctoral Researcher Stage with the Applied Electromagnetism Group, ETSIT-UPM, at the time he was an Adjunct Professor with the EPS-Universidad Autónoma de Madrid. He is currently an Associate Professor and a Researcher with the Radiation Group, Universidad Politécnica de Madrid. In addition, he is being the responsible of the special session on satellite communications systems since its beginnings in URSI2016 until URSI2022 in Spain. He has led and participated in a number of international (ESA, government official and private) projects related to the development of new antenna technologies, ground segment and on-board solutions, and antenna test and validation ranges for the aerospace and defence industry within public and private funding. Besides, he has worked in the design of novel antenna systems and has proposed novel uncertainty analyses methods and calibration methods for active antenna arrays being part of his research interests. Other research areas are related to the analysis, the characterization, and the design of satellite communication antenna systems being the responsible of development of dual-band SATCOM terminals. He is actively involved in the development and design of ultra low-profile antennas for Smallsats including the development of high polarization purity antenna under ESA program. Furthermore, he has participated in the development of algorithms for resource allocation of flexible-transparent transponder systems for classical GEO satellites systems as well as for novel massive LEO satellites constellations and HAP systems. He is currently leading the most significant contributions within European Projects for ESA and Horizon Europe 2020 in the field of Array Processing for Digital Antennas with Beamforming, DoA and Anti-jamming techniques in Satellite Applications. He is currently a member of the Organization, and the Technical and Scientific Committees of the Small Satellites and Services International Forum.

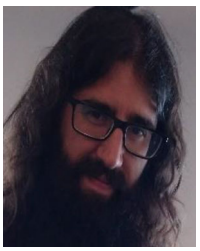

ALVARO ARAUJO PINTO received the degree in Ingeniero Telecomicacion from the Universidad Politécnica de Madrid in 2004, and the Ph.D. degree from the Universidad Politécnica de Madrid in 2007.

He is currently an Associate Professor with the Electronics Engineering Department, Escuela Técnica Superior de Ingenieros de Telecomunicacion de Madrid, where carries out both research and teaching activities. He was a Postdoctoral Researcher with the Berkeley Wireless Research Center, University of California at Berkeley, working in Reliable Radio and a Research stay with BWRC working on human networks in 2018. He is currently the Director of the University-Company Chair Security Direct-Verisure and the Co-Director of the B105 Electronics Systems Lab. He has participated in 70 R+D+I projects funded in competitive tenders by public or private bodies, 21 as a PI during the last eight years. This research has resuṣts in three granted patents in exploitation phase, about 25 scientific publications in high-impact peer-reviewed international journals and more than 30 international and national conferences. His main research and development fields include the development of embedded systems, cognitive radio and wireless neural networks.

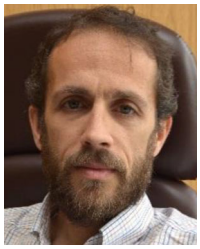

RAMÓN MARTÍNEZ RODRÍGUEZ-OSORIO received the Ph.D. degree in electrical engineering from the Universidad Politécnica de Madrid (UPM), Spain, in 2004.

In 2002, he joined the Telecommunication Engineering School, UPM (ETSIT-UPM), where he has been working as a Full Professor since 2019, and he is member of the Information Processing and Telecommunications Center (IPTC-UPM). Since 2004, he has been a Lecturer with SatCom Systems. In recent years, he has specialized on the optimization of high-throughput satellite systems with the use and operation of flexible payloads using machine learning techniques and the resource allocation problem in LEO satellites equipped with beam-hopping technology. He has led and participated in international projects related to space technology and has collaborated with ESA and space communication companies in technology transfer programs developing antenna array systems and software tools for the optimization of satellite links. He is coordinating a UPM-MIT Aeroastro Department research collaboration aiming to define a system architecting framework for massive LEO constellations. He proposed a novel antenna array design for intersatellite links in nanosatellite missions. He is the Co-Chair of the Technology Working Group of the IEEE LEO SatS Project. His research interests are wireless and satellite communications, the integration of 5G/6G in new NTN systems, and the application of antenna array technology to wireless systems.

MANUEL SIERRA PÉREZ (Life Senior Member, IEEE) was born in Zaragoza. He received the degree in telecommunications engineer from the Polytechnic University of Madrid in 1975, and the Doctoral degree from the Polytechnic University of Madrid in 1980.

He has been a University Professor with the Department of Signals, Systems and Radiocommunications, Polytechnic University of Madrid since January 1990. Retired In 2019, he has been a Professor Emeritus with UPM since January 2020. He has given courses and already teach on antennas, communication electronics, electromagnetism and microwave circuits in the titles of graduate, master, and doctorate in telecommunication engineering. His research field covers the design of antennas and radiofrequency circuits associated to the antenna systems. In the last years has been involved in the study and design of active antenna systems for communications, radar and control systems.

Prof. Pérez has been the President of the IEEE Spain Section, Spanish delegate in the European Cost actions Cost 260, Cost 284, Cost 603, and Cost Ic-1002 Vista, a member of the URSI Spanish Committee, and the President of the Spanish Antenna Network and Spanish delegate of the European Association of Antennas and Propagation of Waves (EurAAP). He has been the President of the National URSI Symposium in Madrid 1996 and the President of the European Congress of Antennas and Wave Propagation (EuCAP) in Barcelona 2010.